

Research Paper



Middle and Late Holocene paleolimnological changes in central Lake Tanganyika: Integrated evidence from the Kavala Island Ridge (Tanzania)

The Holocene I–14 © The Author(s) 2024
Article reuse guidelines:
sagepub.com/journals-permissions
DOI: 10.1177/09596836241254475
journals.sagepub.com/home/hol



Leandro Domingos-Luz, Dichael J Soreghan, Siliane G Rasbold, Geoffrey S Ellis, Justin E Birdwell, Ishmael A Kimirei, Christopher A Scholz and Michael M McGlue

Abstract

Middle and Late Holocene sediments have not been extensively sampled in Lake Tanganyika, and much remains unknown about the response of the Rift Valley's largest lake to major environmental shifts during the Holocene, including the termination of the African Humid Period (AHP). Here, we present an integrated study (sedimentology, mineralogy, and geochemistry) of a radiocarbon-dated sediment core from the Kavala Island Ridge (KIR) that reveals paleoenvironmental variability in Lake Tanganyika since the Middle Holocene with decadal to centennial resolution. Massive blue-gray sandy silts represent sediments deposited during the terminal AHP (~5880–4640 cal yr BP), with detrital particle size, carbon concentrations, light stable isotopes, and mineralogy suggesting an influx of river-borne soil organic matter and weathered clay minerals to the lake at that time. Enhanced by the AHP's warm and wet conditions, chemical weathering and erosion of Lake Tanganyika's watershed appears to have promoted considerable nutrient recharge to the lake system. Following a relatively gradual termination of the AHP over the period from ~4640 cal yr BP to ~3680 cal yr BP, laminated and organic carbonrich sediments began accumulating on the KIR. $\delta^{15}N_{\text{bulk}}$, C/N, and hydrogen index data suggest high relative primary production from a mix of algae and cyanobacteria, most likely in response to nutrient availability in the water column under a cooler and seasonally dry climate from ~3680 to 1100 cal yr BP. Sediments deposited during the Common Era show considerable variability in magnetic susceptibility, total organic carbon content, carbon isotopes, and C/N, consistent with dynamic hydroclimate conditions that affected the depositional patterns, including substantial changes around the Medieval Climate Anomaly and Little Ice Age. Data from this study highlight the importance of sedimentary records to constrain boundary conditions in hydroclimate and nutrient flux that can inform long-term ecosystem response in Lake Tanganyika.

Keywords

African Great Lakes, African humid period, hydroclimate, paleoenvironment

Received 3 October 2023; revised manuscript accepted 22 March 2024

Introduction

Transitions between hydroclimate states have significant implications for watershed evolution, lake ecosystem processes, and human communities, as rapid shifts can lead to disruptions in habitats and ecosystem services, and cause migrations of animals and people (Cohen et al., 2006; Tierney et al., 2010a; Yost et al., 2021). Lake Tanganyika, located in the East African Rift System (EARS), houses one of the longest and most continuous continental sedimentary archives of hydroclimate and ecological change for the Afro-tropics (Russell et al., 2020). The lake likely began accumulating sediment in the Miocene, and its deep anoxic bottom waters are often ideal for preserving finely laminated sediments with seasonal to centennial temporal resolution (Cohen et al., 2006; Ivory and Russell, 2016; McGlue et al., 2020). Yet given its great size, remote location, and complex limnogeology, sedimentary records spanning even major periods of Holocene environmental instability on the African continent remain unsampled or understudied at Lake Tanganyika.

In Africa, one of the most profound Holocene hydroclimate transitions is the termination of the African Humid Period (AHP), when warm and wet conditions from the latest Pleistocene shifted to drier conditions after ~5000 calibrated years before present day (cal yr BP) across much of the continent (Ivory and Russell, 2018;

Department of Earth and Environmental Sciences, University of Kentucky, USA

Corresponding author:

Leandro Domingos-Luz, Department of Earth and Environmental Sciences, University of Kentucky, 121 Washington Ave, Lexington, KY 40506, USA.

Email: leandro.luz@uky.edu

²School of Geosciences, University of Oklahoma, USA

³U.S. Geological Survey, Central Energy Resources Science Center, USA ⁴Tanzania Fisheries Research Institute, Tanzania

⁵Department of Earth and Environmental Sciences, Syracuse University,

Shanahan et al., 2015). The AHP was mainly driven by changes in insolation in the Northern Hemisphere that culminated in a largescale expansion of the African monsoon system (Shanahan et al., 2015) due to the influx of Atlantic moisture and enhanced convergence along the Congo Air Boundary (Tierney et al., 2011). During this wet paleoclimate phase, the Sahara Desert was transformed into an open savannah, with patches of woodland and myriad shallow lakes supporting abundant fauna and widespread huntergatherer settlements (DeMenocal and Tierney, 2012; Tierney et al., 2011). At Lake Tanganyika, the timing of the termination of the AHP and the importance of this transition to paleolimnology, ecosystem change, and deepwater sedimentation need to be better resolved, and this study seeks to fill this gap. This is because most Middle Holocene records recovered from the basin have been limited by low temporal resolution or constrained by depositional hiatuses (Kamulali et al., 2022; Tierney et al., 2011).

In this paper, we present multiple sedimentological, geochemical, and mineralogical indicators from a sediment core retrieved in the Kavala Island Ridge (KIR) in central Lake Tanganyika that provide a more comprehensive timeline and a high-resolution picture of the response of Lake Tanganyika to the termination of the AHP. Our results highlight the importance of the AHP for nutrient loading in Lake Tanganyika, which helped to shape patterns of primary production in the middle and Late-Holocene. The study shows evidence for variable environmental conditions following the gradual transition out of the AHP, with diminished influence from high riverine discharge, chemical weathering, and erosion on KIR sedimentation.

Study area

Lake Tanganyika (3°–9°S latitude, 29°–30° E longitude) occupies a series of half-graben rift basins in the western branch of the East African Rift System, separated by zones of overlapping basinbounding border faults (Figure 1; Rosendahl, 1987). Lake Tanganyika is the second deepest ($Z_{mean} = 570 \, m; Z_{max} = 1400 \, m$) lake in the world and supports the second most productive pelagic fishery in Africa (McGlue et al., 2008; O'Reilly et al., 2003). The lake stretches ~650 km along its north-south axis and up to 80 km in the east-west direction (Degens et al., 1971). The watershed geology consists of Proterozoic gneisses and other metasedimentary rocks, with minor Neogene-Quaternary volcanic basalts in the northernmost part of the basin (Tiercelin and Mondeguer, 1991). Classified as a meromictic lake, Lake Tanganyika is permanently stratified with an anoxic hypolimnion below ~150 m water depth, but the depth of this boundary is known to vary spatially, and it has been influenced by anthropogenic global warming (Cohen et al., 2016). During the austral winter, strong southerly winds result in the upwelling of deep cold, P- and Si-rich waters to the photic zone, driving primary production (Degens et al., 1971; McGlue et al., 2020; O'Reilly et al., 2003). Upwelling dynamics during the Late Holocene are associated with the effects of solar irradiance, lake surface warming, and El Niño Southern Oscillation on monsoon wind strength (McGlue et al., 2020).

Because of its size, precipitation patterns vary along the length of Lake Tanganyika, which results from the seasonal migration path of the tropical African rain belt, influenced by mesoscale convective systems (Nicholson, 2022). The highest rainfall in the lake's watershed occurs in the northern highlands in two wet seasons, from March to May and September to December, yielding precipitation >1600 mm/yr. The lowest rainfall occurs in the southern part of the lake, in a single rainy season from November through March, with precipitation <870 mm/yr (Ivory and Russell, 2016). Riverine discharge and groundwater flux to Lake Tanganyika are relatively low, and rainfall accounts for most of the water input (Tiercelin et al., 1992). Lake Kivu is hydrologically connected to Lake Tanganyika, entering from the north via the

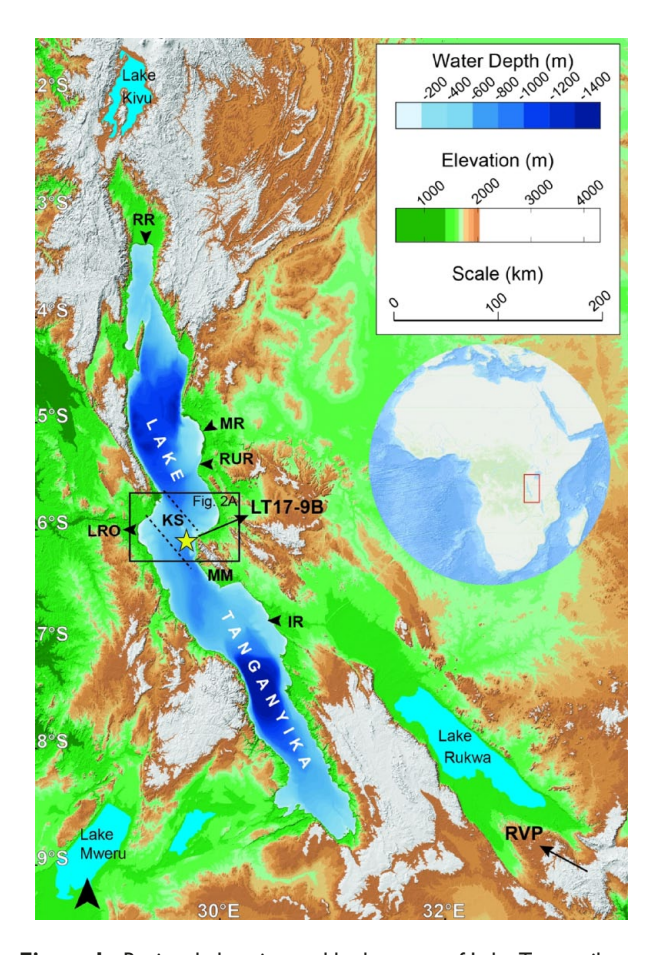


Figure 1. Regional elevation and bathymetry of Lake Tanganyika. Core 9B was retrieved from ~420 m water depth (5.95290°S, 29.63970°E) on the Kavala Island Ridge (KIR) crest (also known as the Kalemie Shoal, KS). The inset map shows the location of Lake Tanganyika in Africa, and the black rectangle denotes the location of the inset map in Figure 2a. MM: Mahale Mountains; RR: Ruzizi River; MR: Malagarasi River; RUR: Rugufu River; IR: Ifume River; LRO: Lukuga River outlet; RVP: Rungwe Volcanic Province.

Ruzizi River; the Ruzizi is also a major contributor of salts and carbonates (Cohen et al., 1997a). Another significant tributary is the Malagarasi River, which enters the lake on the eastern shore (Vincens, 1991). The hydrological outputs are dominated by evaporation, and the Lukuga River is the only outlet, which drains into the Congo River basin to the west (Degens et al., 1971).

Kavala Island Ridge

The Kavala Island Ridge (KIR) is an important sub-lacustrine geomorphological feature in central Lake Tanganyika; it is an uplifted basement horst block that forms a perched depositional environment (Figure 2). The KIR is the offshore extension of the Mahale Mountains, created by an NW-SE striking normal fault of the Kigoma Basin (Scholz et al., 2003). This feature, referred to in some publications as the Kalemie Shoal, is a heterogeneous bedrock spine with a relatively thin veneer of lake sediment cover (Scholz et al., 2003). Sediment accumulation is reported to occur chiefly through the slow gravitational settling of organic-rich detritus, promoting some of the basin's lowest sedimentation rates (Tiercelin et al., 1992). Seismic reflection data indicate that the KIR was subaerially exposed during extreme water-level lowstands (>300 m) (Shaban et al., 2021), dividing the lake at those times, which very likely has contributed to speciation and the evolution of Lake Tanganyika's spectacular biodiversity (Vanhove et al., 2015). The positive relief above the lake floor produced by the KIR precludes the influence of erosive gravity flows

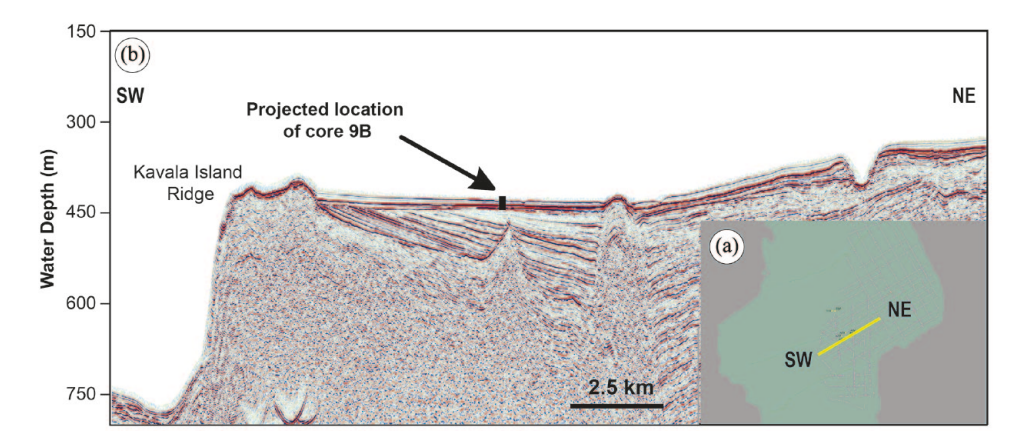


Figure 2. Single-channel seismic reflection profile of the Kavala Island Ridge (KIR). (a) Inset map shows the relative position of the seismic line in central Lake Tanganyika (see Figure 1 for spatial reference). (b) Southwestnortheast oriented seismic profile illustrating the morphology of the KIR and projected location of core 9B. The vertical scale is in two-way travel time (milliseconds) converted into water depth, considering a travel time of 1500 m/s. Seismic data are from Scholz et al. (2003). Core location illustrates the isolated high-relief region of Lake Tanganyika that experiences slow sedimentation rates.

Table 1. Reservoir-corrected radiocarbon dates were used to construct the age-depth model.

CAMS#	Depth (cm)	Material	Age (¹⁴ C)	Error	Reservoir Offset (yrs)	Reservoir-corrected age (14C)
177509	ı	SOM	915	30	965	-50 (post-bomb)
180927	13.5	SOM	1095	30	920	180
186545	17	SOM	1135	45	905	230
177510	28	SOM	1150	30	800	750
180928	39.5	SOM	1950	30	700	1250
186546	47	SOM	1685	45	765	920
177511	49	SOM	2130	30	650	1480
186543	67	SOM	2760	45	470	2290
177512	69	SOM	4145	30	420	3730
180929	79.5	SOM	3450	30	445	3010
177513	89	SOM	2925	30	465	2460
180930	94.5	SOM	4325	30	410	3920
186544	99	SOM	4950	45	340	4560
186547	102	SOM	2525	45	480	2050
177517	105	SOM	5620	35	365	5260

SOM: sedimentary organic matter; CAMS#: Center for Accelerator Mass Spectrometry number.

that are common elsewhere in Lake Tanganyika, making sediment cores from this environment particularly attractive for obtaining more complete records of environmental change.

Previous studies of the KIR utilized sediment cores collected with a heavy marine-type vibracorer that recovered Pleistocene-aged sediments (Scholz et al., 2003). For example, the well-studied T97-52V core helped to show that a series of droughts profoundly altered the water cycle across a broad swath of sub-Saharan Africa nearly 100,000 yr BP (Scholz et al., 2007). Geochemical datasets from the T97-52V core have revealed broad, millennial-scale changes in organic matter production and detrital particle size, including key shifts around the Last Glacial Maximum related to lowering water levels (Burnett et al., 2011). In contrast, Middle and Late Holocene records from the KIR have been unavailable.

Material and methods

Sediment core

The sediment core analyzed in this study (LT-TANG17-9B-1U-1, hereafter core 9B) was retrieved from the KIR crest (5.95290° S, 29.63970° E) using a lightweight UWITEC gravity corer deployed from the *M/V Maman Benita* in 2017. The coring site is located ~14 km offshore in ~420 m of water. Standard handling procedures

were applied during collection, and the core was shipped to the Continental Scientific Drilling Facility at the University of Minnesota (USA) for analysis. Core 9B was scanned for physical properties using GEOTEK MSCL-S and XYZ tools, split, and photographed at high resolution. The core description followed the classification scheme proposed by Schnurrenberger et al. (2003), focusing on macroscopic structures (e.g. bedding features, texture, color) and the microscopic identification of major and minor sedimentary components. Sub-samples for discrete analyses were collected every centimeter (n=105). The physical property employed in this study was magnetic susceptibility (MS), which is used to trace ferromagnetic grains in lake sediments and is often an indicator of terrigenous inputs (Thompson et al., 1975).

Geochronology

Core 9B was radiocarbon (¹⁴C) dated along 14 horizons (Table 1) using fine-fraction sedimentary organic matter (SOM) at the Center for Accelerator Mass Spectrometry at Lawrence Livermore National Laboratory (Livermore, CA). The sediment samples were pre-treated using sequential acid-base-acid digestion to remove potential modern contaminants. The insoluble material was dried overnight at low temperature and transferred into a glass tube, where silver and copper were added before conversion

to CO2 and then graphite for 14C measurement by accelerator mass spectrometry. 14C dating of Holocene sediments from Lake Tanganyika is challenging due to old carbon in the dissolved inorganic carbon pool, leading to a reservoir effect. One approach to address this issue involves pairing bulk sedimentary organic matter with terrigenous plant remains from the same stratigraphic horizon (Felton et al., 2007). However, the absence of terrigenous plant remains in the KIR sediments made this approach impossible for core 9B. To overcome this limitation, we utilized the regression equations provided by Felton et al. (2007) to estimate the reservoir effect prior to constructing the age model in Bacon age-modeling software. Felton et al. (2007) observed that age offsets were the largest in the Late Holocene and thus developed two separate regression equations. We used those two regression equations, one for ages $\leq 2500 \,\text{yr}$ BP (y=-0.2576x+1200.2; $R^2 = 0.72$) and another for ages > 2500 yr BP (y = -0.0373x + 572.5; R^2 =0.99). The R-based package ("rbacon") was used to construct the final age-depth model, taking advantage of Bayesian statistics to reconstruct the sediment accumulation history (Blaauw and Christen, 2011). The reservoir-corrected ages were calibrated using the SHCal13 calibration curve (Hogg et al., 2013), and all results and interpretations are based on the median calibrated age (cal yr BP). We acknowledge that additional paired ages, particularly in the Late Holocene where age offsets are the largest, will help to improve future radiocarbon-based chronology.

Geochemistry

Geochemical analyses on core 9B included total organic carbon (TOC), total nitrogen (TN), $\delta^{13}C_{org}$, $\delta^{15}N_{bulk}$, hydrogen index (HI), and oxygen index (OI) (n=105). The TOC and $\delta^{13}C_{org}$ were measured at the U.S. Geological Survey (USGS) using a LECO 744 carbon analyzer (Oliver and Warden, 2020) and an elemental analyzer connected to an isotope ratio mass spectrometer (French et al., 2023), respectively. To remove inorganic phases, samples were pre-treated with dilute HCl prior to TOC and $\delta^{13}C_{org}$ measurements. Quality control procedures for TOC measurements included the use of calibration and check standards as well as sample duplicates in each batch. The precision of the $\delta^{13}C_{org}$ measurement, established by repeat measurements of internal standards, was 0.02‰, and each sample was analyzed in duplicate. All carbon isotope results were calibrated to the Vienna Pee Dee belemnite scale. The TN and $\delta^{15} N_{\text{bulk}}$ were measured at the University of Tennessee (Knoxville); the TN dataset was used in conjunction with the TOC to calculate the C/N, with values expressed as atomic ratios (Meyers and Ishiwatari, 1993). Samples that underwent isotope ratio mass spectrometry analysis for $\delta^{15}N_{\text{bulk}}$ were not pre-treated and, therefore, represent N from bulk sediment, which we assume is chiefly derived from organic matter HI and OI data were determined by the USGS using a Hydrocarbon Analyzer with Kinetics (HAWK) programed pyrolysis instrument running version R8355 software (Wildcat Technologies) (Dreier and Warden, 2021). Values of HI were calculated from the S2 pyrolyzate fraction (mg-hydrocarbon/g-rock) normalized to TOC. The OI is derived from the S3 pyrolyzate fraction (mg-CO₂/grock) normalized to TOC. These data are approximately proportional to H/C and O/C ratios, respectively, and they are used here as indicators of the provenance of organic matter along with the C/N data (Orr, 1981; Peters, 1986). Quality control for programed pyrolysis results included calibration and laboratory check standards and duplicate sample analysis conducted every 20 samples. All data generated by the USGS for this study are available in a data release available at ScienceBase.gov (Birdwell et al., 2024).

Micro X-ray fluorescence and mineralogy

Micro X-ray fluorescence (µXRF) measurements were performed at 0.2 mm spatial resolution using an ITRAX core scanner at the

Large Lakes Observatory (University of Minnesota-Duluth), with a Cr X-ray source tube at 30 kV and 55 mA with a 15-s dwell time. The µXRF core scanner provides a nondestructive analysis of elements from aluminum to uranium. Mineralogy was inferred using non-destructive attenuated total reflectance (ATR) Fourier-transformed infrared spectroscopy (FTIR). The ATR-FTIR measurements were conducted at the USGS following the methods described in Washburn and Birdwell (2013); dried samples were ground to a uniform 60-mesh, and approximately 10 mg was measured on a Bruker Alpha spectrometer equipped with an attenuated total reflectance module containing a diamond internal reflection element (Murphy et al., 2020). Quality control included running protocols recommended by the manufacturer that included analysis of a polystyrene instrument standard as well as laboratory check standards and sample duplicates. Spectra were interpreted using the multivariate curve resolution tool in The Unscrambler X (ver. 10.5.1; CAMO Software) as described in Gall et al. (2022).

Clastic mass fraction and particle size analysis

Using methods from Burnett et al. (2011), ~1 g of wet sediment was lyophilized, weighed, and treated to remove labile organic matter, carbonate, and opal with 30% hydrogen peroxide, 1N hydrochloric acid, and 2M sodium carbonate, respectively. Samples were rinsed and centrifuged between each treatment. The samples were then freeze-dried and weighed again. The clastic mass fraction was determined by subtracting the percent mass loss from 100. Smear slides were used to check for organic matter, carbonates, and/or diatoms; the process was typically successful, although micro-charcoal and sponge spicules (<2%) occasionally remained.

For grain-size characterization, the freeze-dried siliciclastic sample was wetted and placed in a sonicator for 10 min. Dispersant was added, and a small pipette was used to draw a representative sample from the slurry. The full aliquot was introduced into a Malvern Mastersizer 3000 using a Hydro SM small volume module set at 2500 rpm; the acceptable obscuration range was 15–24%. Adding the full aliquot lessened the chance of grain size separation within the pipette. Reported here are the relative proportions of sand (>63 μ m), silt (<63 and >4 μ m), and clay (<4 μ m) by volume.

Statistical analyses

To reduce the dimensionality of the different datasets, we applied a principal component analysis (PCA) on the MS, TOC, C/N, $\delta^{13}C_{org}, \delta^{15}N_{bulk}, \% clay, \% silt, \% sand, \% detrital, HI, and OI, using the software PAST (Hammer et al., 2001). The PCA helped to identify downcore trends and depositional units.$

Results

Stratigraphy and age modeling

Radiocarbon geochronology (¹⁴C) of core 9B spans from the Late Middle Holocene (~5880 cal yr BP) to ~2000 CE (post-bomb; 50 years after 1950), indicating that the top of the core was minimally disturbed during sampling (Table 1; Figure 3). The Bacon model excluded four outliers from the age-depth solution. Most outliers exhibit spuriously young ages, which we attribute to modern carbon contamination or ineffective chemical pretreatments. Conversely, one outlier displayed an anomalously old age, which may have resulted from the release of stored organic material from the landscape by erosion, a process that has been inferred elsewhere (e.g. Olsson, 1991). Interestingly, the sample with the anonymously old age was not within Units I-a or I-b, as might be anticipated to accompany the erosive landscape of the AHP. The mean long-term accumulation rate of core 9B is ~0.017 cm yr⁻¹,

highlighting the low sedimentation rates on the KIR. The sedimentation rate in the sediments from the AHP (~5880–4640 cal yr BP) was considerably slower (~0.006 cm yr⁻¹) compared to the

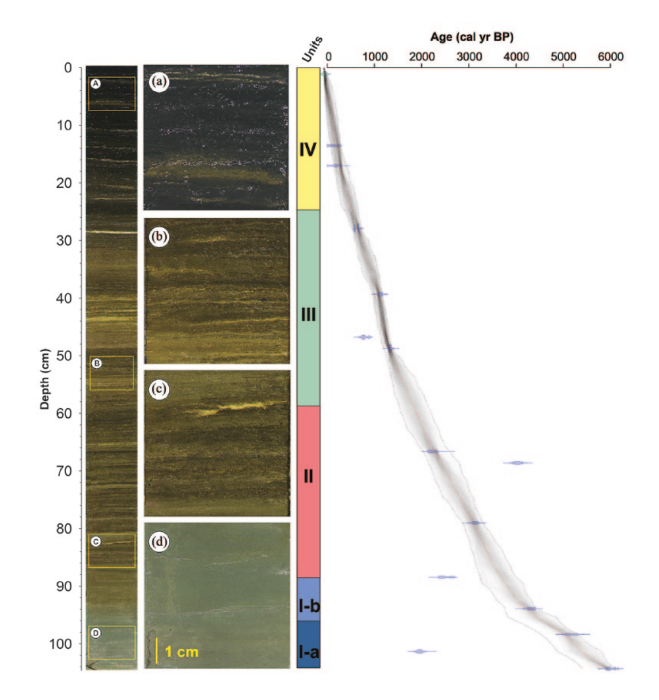


Figure 3. High-resolution core photograph, lithostratigraphic units (I–IV, oldest to youngest, respectively), and age-depth model of core 9B. Detail figures are ∼6 cm thick and representative of each lithostratigraphic unit. (a) Unit IV sapropel with laminae of diatomaceous ooze. (b) Unit III brown clayey silt with mm-scale laminae of diatomaceous ooze or carbonate (white). (c) Unit II light brown clayey silt laminae encasing a thin discontinuous tephra. (d) Unit I-a and Unit I-b consist chiefly of massive sediments. In the age-depth model, blue markers represent reservoir-effect calibrated ¹⁴C dates, the red line denotes the best-fit solution, and the gray shading indicates the 95% confidence interval.

rest of the core (~0.02 cm yr^-l). A thin, wispy, and buff-colored layer was found at 83 cm down core; volcanic glass and a K/Ti peak in the μXRF dataset suggest this feature is a tephra layer (Supplemental Materials; Figure S1). The age model places this candidate tephra layer at ~3580–3030 cal yr BP within the 2σ error range.

Based on sediment composition, the nature of bedding/contacts, and MS patterns, core 9B was divided into four sedimentary units (Figure 3).

Unit I-a (105–97 cm; ~5880–4640 cal yr BP). Unit I-a consists of massive blue-gray sandy silts exhibiting intermediate MS values (Figures 3 and 4). Unit I-a sediments have variable percentages of clastic detritus (~52.4–85.6%) with a mean of 80.5% (Figure 3). In Unit I-a, silt>sand>clay, with mean values of 51%, 38%, and 11%, respectively. Unit I-a sediments exhibit relatively uniform values of TOC and TN moving upward from the basal contact (~4.5–5.6 wt.% and ~0.30–0.37 wt.%, respectively). C/N, HI, and OI vary very little in Unit I-a (Figure 4). The δ^{13} C or values range from –24.7 % to –23.9 %, while values of δ^{15} N bulk are relatively high, ranging between ~1.7 and 2.1 %. The FTIR data suggest relatively abundant amorphous kaolinite and illite-muscovite in the Unit I-a clay minerals, as well as low quartz and crystalline kaolinite (Figure 5).

Unit I-b (97–89 cm; ~4640–3680 cal yr BP). Unit I-a grades into Unit I-b, which consists of gray-brown faintly laminated mud with a long-term declining trend in MS (Figures 3 and 4). Unit I-b sediments have highly variable percentages of clastic detritus (~21.5–81.6%), abundant silt (mean of ~58%), highly variable sand (~0.3–75%), and clay content (~1.1–55%). Unit I-b exhibits increasing trends from the basal to the upper contact in TOC, HI, OI, and $\delta^{13}C_{\rm org}$ (Figure 4), whereas C/N declines toward the upper contact. Unit I-b has $\delta^{13}C_{\rm org}$ values that range from ~25.8% to ~23.1% (mean = ~24.4 %). A prominent change in Unit I-b is in $\delta^{15}N_{\rm bulk}$, which declines considerably relative to the underlying unit. The $\delta^{15}N_{\rm bulk}$ decreases toward the top of the unit, with a mean of 0.6%. The FTIR data indicate

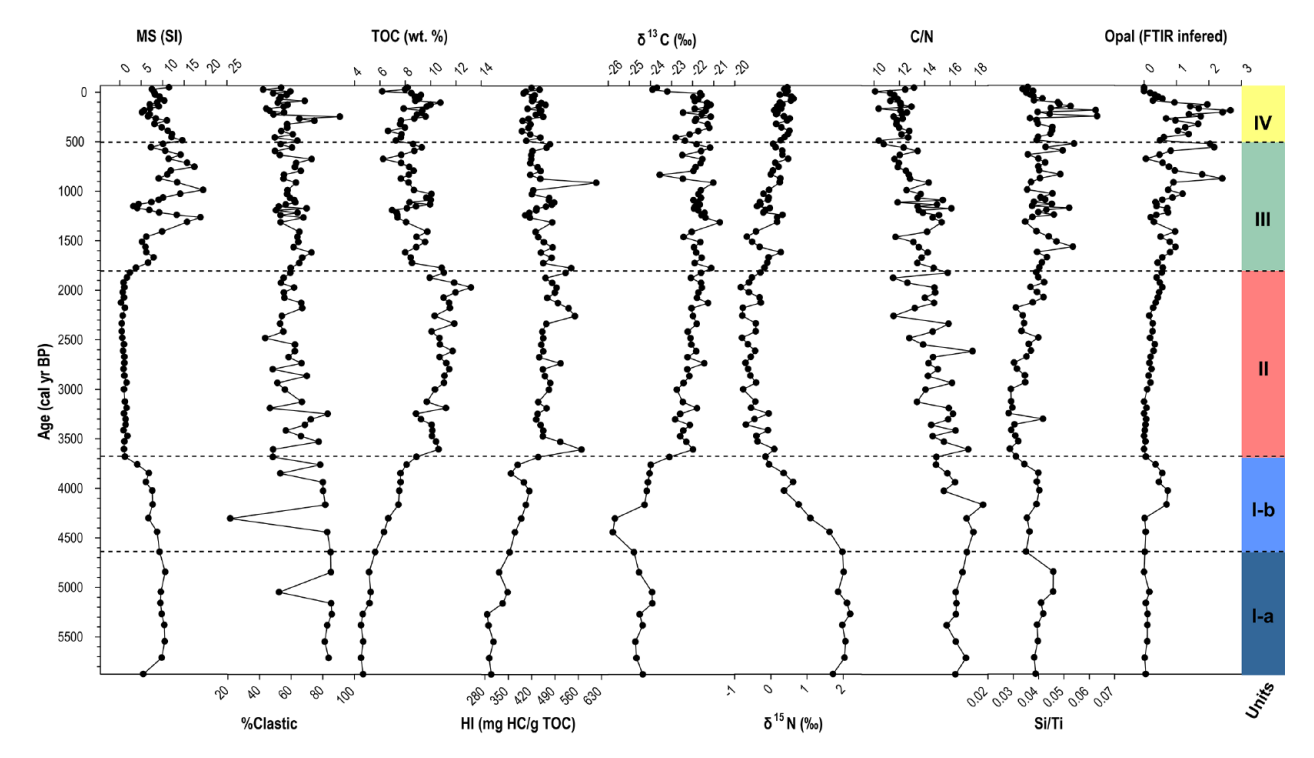


Figure 4. Chemostratigraphy of core 9B. Magnetic susceptibility (MS), %clastic content, total carbon content (TOC), hydrogen index (HI), stable isotope of carbon ($\delta^{13}C_{orp}$) and nitrogen ($\delta^{15}N_{bulk}$), C/N, Si/Ti (μ -XRF), and FTIR-inferred opal content.

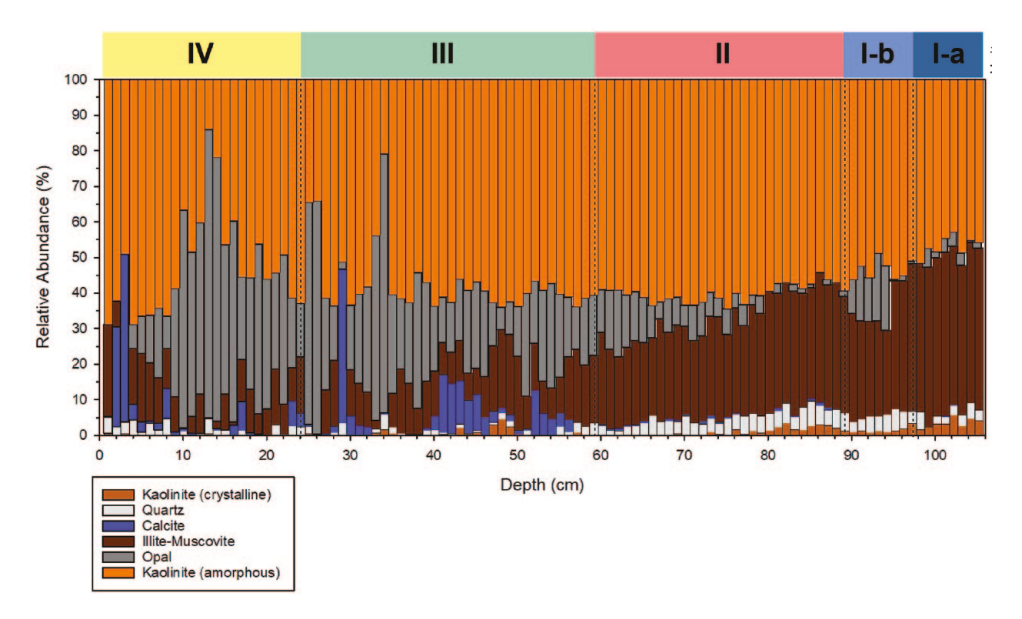


Figure 5. Fourier-transform infrared spectroscopy analysis of core 9B. Relative abundance reflects component weights from multivariate curve analysis of sediment spectra.

relatively abundant amorphous kaolinite and illite-muscovite clay minerals, as well as an increase in opal relative to Unit I-a (Figure 5).

Unit II (89–59 cm; ~3680–1820 cal yr BP). Unit II sediments contain organic-rich, laminated silts with low MS (Figures 3 and 4). Laminations are typically flat and laterally continuous, apart from a wispy, discontinuous layer with chemical characteristics consistent with volcanic ash (Supplemental Materials; Figure S1). Clastic detritus content in Unit II is highly variable, ranging from 43.6% to 83.1%. Compared to Unit I-b, there is an increase in siltsized grains (mean=~66%) and a decline in clay (mean=~11%). Unit II exhibits uniformly high values of TOC (mean = 10.8 wt.%; range=8.9-13.2 wt.%). HI shifts to higher values at the base of Unit II and varies a little around a mean of ~475 mg hydrocarbon/g TOC, while the mean OI is ~43 mg CO₂/g TOC (Figures 4 and 6). Similar to HI, the $\delta^{13}C_{org}$ shifts to more positive values at the base of Unit II, then varies little moving toward the upper contact (range of -22.8 to -21.2%), while $\delta^{15}N_{bulk}$ exhibits the opposite trend, shifting toward more negative values near the basal contact (0.1 to -0.8%; Figure 4). C/N is highly variable in Unit II, with values ranging between 11 and 18. The FTIR data suggest abundant amorphous kaolinite but a decreasing trend in illite-muscovite toward the top of the unit. Opal detections increase toward the top of Unit II (Figure 5).

Unit III (59–25 cm; ~1820–520 cal yr BP; ~130–1430 CE). Unit III consists of laminated sandy silt with occasional carbonate laminae. Laminations in Unit III range from flat, parallel, and continuous to slightly tilted and discontinuous. MS values exhibit high amplitude variations that distinguish this unit from Unit II (Figures 3 and 4), with peaks at 48, 36, and 31 cm depth, corresponding to ~1200 cal yr BP (~750 CE), ~1000 cal yr BP (~950 CE), and 700 cal yr BP (~1250 CE), respectively. Unit III sediments show variable percentages of clastic detritus (mean=60.6%; range=49.8–72.9%) with high and widely varying silt (mean=~68%) and sand content (mean=~22%; Figure 7). TOC and TN concentrations decline slightly relative to Unit II; high values of these proxies usually align with low values of MS. The mean HI for Unit III is ~453 mg hydrocarbon/g TOC, and the mean OI is ~42 mg CO₂/g TOC. Values of $\delta^{13}C_{org}$

are very similar to Unit II (mean=-21.8%), whereas $\delta^{15}N_{bulk}$ increases to a mean of 0.0%. The mean C/N (13) declines slightly relative to the underlying unit and shows less variability. FTIR data suggest a substantial increase in opal and calcite, whereas quartz becomes rarer and illite shows a declining trend toward the upper contact (Figure 5).

Unit IV (25–0 cm; \sim 520 – \sim 50 cal yr BP; \sim 1430–2000 CE). Unit IV sediments consist of diatom-rich sapropel with occasional carbonate laminae near the basal contact and low MS relative to Unit III (Figures 3 and 4). Unit IV exhibits highly variable clastic content (~42.3–90.8%) with a mean of 68.1%. The silt size fraction (mean=68.1%) dominates, followed by variable sand (~0-70%) and low clay (~2.5-27%) content. Unit IV exhibits intermediate and variable TOC and intermediate to high TN values (\sim 6.1–10.7 wt.% and \sim 0.6–1.0 wt.%, respectively). The mean HI value is ~425 mg hydrocarbon/g TOC and the mean OI is ~46 mg CO₂/g TOC. Sediments from Unit IV have $\delta^{13}C_{org}$ values that range from -23.9 to -21.1% and $\delta^{15}N_{bulk}$ from 0.1 to 0.6%. The C/N mean declines slightly to ~12. In Unit IV, opal and amorphous kaolinite dominate the FTIR-inferred mineralogy except at the top of the record, where illite relative abundance exceeds that of opal (Figure 5).

Principal-component analysis (PCA)

The first principal component (PC1) accounts for ~40% of the variance in the dataset (Figure 8). Unit I and II samples load on opposite sides of the PC1 axis. Samples from Units I-a and I-b load positively on PC1, associated with elevated values of MS, C/N, %clastic, $\delta^{15}N_{\rm bulk}$, and OI. In contrast, samples from Unit II display lower values of PC1, associated with relatively high values of TOC, HI, and $\delta^{13}C_{\rm org}$. Units III and IV load close to the origin of the PC1 axis. The second principal component (PC2) accounts for ~20% of the variance in the dataset. PC2 is primarily associated with changes in grain size and is positively associated with higher %silt and %clay and with lower %sand and %clastic. Unit I-b is prominent on the PC2 plot, with dominantly positive values, whereas Units II and III exhibit the most negative PC2 values (Figure 8, Table S1 and S2 in the Supplemental Information).

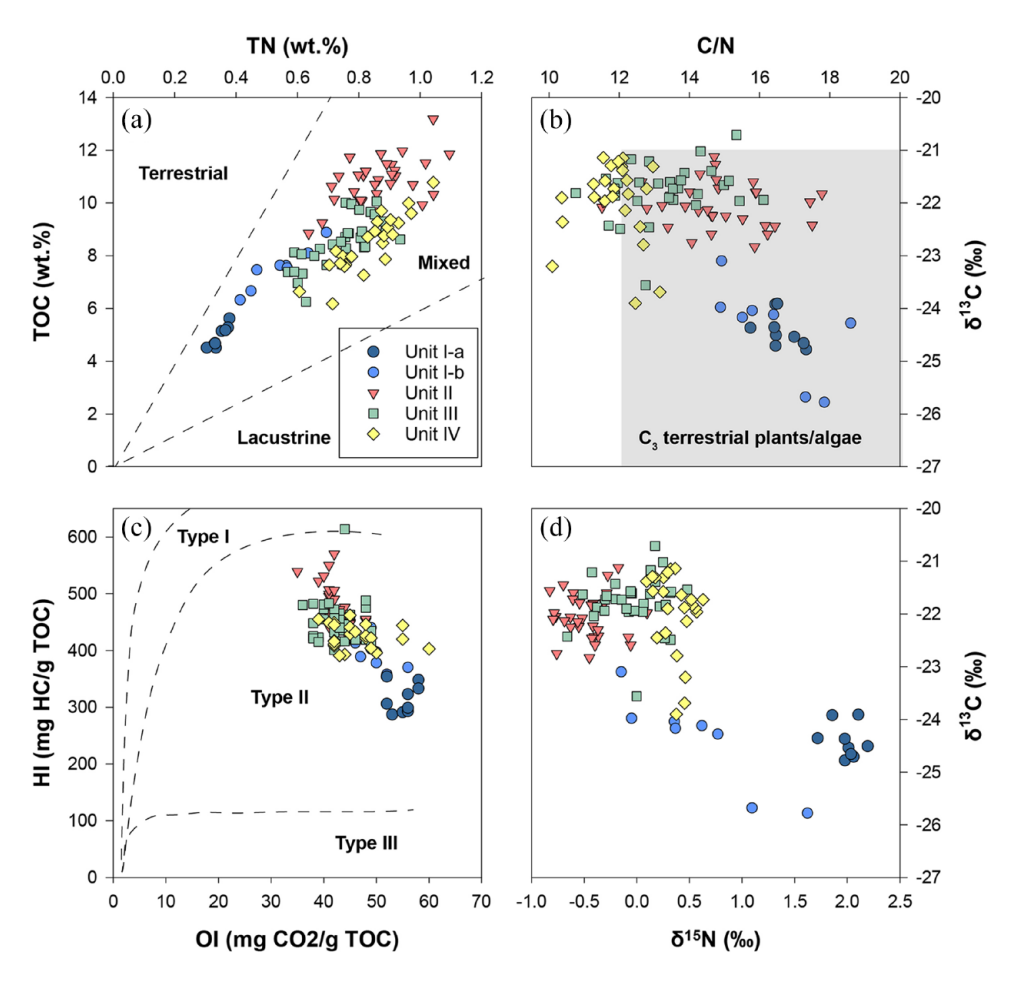


Figure 6. Geochemical data cross-plots by lithostratigraphic units of core 9B. (a) total organic carbon (TOC; wt.%) versus total nitrogen (TN; wt.%); (b) $\delta^{13}C_{org}$ (%) versus C/N values; (c) hydrogen index (HI; mg hydrocarbon/g TOC) versus oxygen index (OI; mg CO₂/g TOC); (d) $\delta^{13}C_{org}$ (%) versus bulk $\delta^{15}N_{bulk}$ (%).

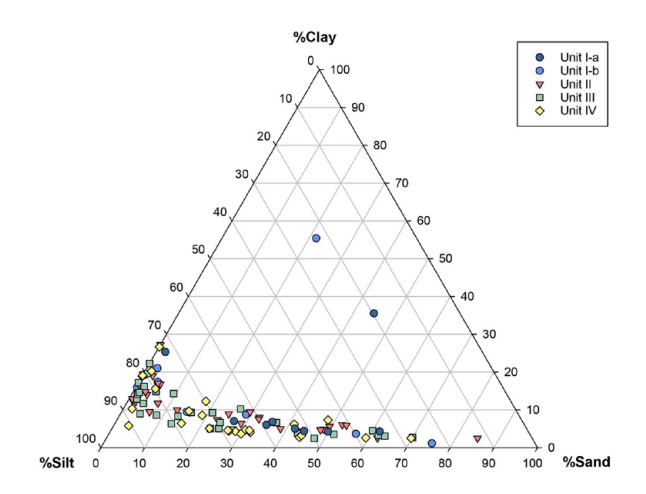


Figure 7. Grain size distribution of core 9B by lithographic unit. Most samples are composed of silt, sandy silt, and silty sand. The highest percentages of clay are in Unit I.

Discussion

Stratigraphy and geochronology

Our integrated record from core 9B suggests that limnological and hydroclimatic fluctuations affected the deposition patterns on the KIR over the past ~5880 cal yr BP. Given the ¹⁴C age-depth model, the core 9B record offers multi-decadal to centennial temporal resolution between samples. Core 9B was retrieved from near the crest of the KIR deepwater horst, and the stratigraphy of

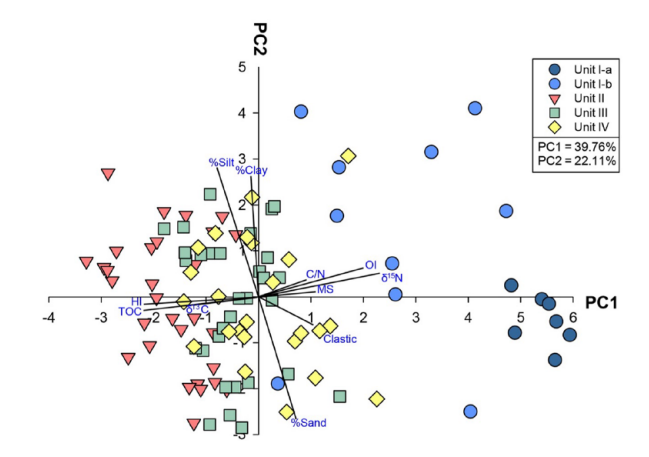


Figure 8. Principal component analysis (PCA) of geochemical and grain size data from core 9B. Combined, PC1 and PC2 account for ~62% of the variance in the dataset. Variables used include magnetic susceptibility (MS), organic matter proxies (total organic carbon, TOC; total nitrogen, TN; C/N ratio; hydrogen index, HI; oxygen index, OI), light stable isotope geochemistry ($\delta^{13}C_{org}$, $\delta^{15}N_{bulk}$), and grain size (%clay, %silt, %sand, %clastic).

the core is consistent with a depositional setting free from the influence of gravity flows. Therefore, we assume the core sediments are derived chiefly from particles settling from suspension in the water column onto the lake floor with minimal influence of erosion. This depositional setting produces relatively slow sedimentation rates $(0.01 \text{ cm yr}^{-1})$, similar to other deep-water horsts

Table 2. Summary of indicators in Lake Tanganyika sediments. These interpretations are generalized and based on our integrated data; exceptions can be found in other lake systems.

Wetter

Higher MS and %clastic

Increased runoff and terrigenous input.

Lower TOC

Enhanced organic matter decomposition or reduced preservation potential. On its own, does not necessarily indicate wet conditions.

Higher TN and $\delta^{15}N_{bulk}$

Increased nutrient input from external sources

High C/N

Higher contribution of terrigenous organic matter. Coupled with low $\delta^{\rm 13} C$ values may indicate an increased influence of terrigenous C_3 vegetation and enhanced precipitation.

More negative $\delta^{\rm I3}{\rm C}_{\rm org}$

Indicates a greater proportion of C_3 vegetation from the landscape or decreased algal productivity within the lake.

Lower HI

Presence of lignin-derived material and less hydrogen-rich compounds. On its own not necessarily indicate wet conditions.

Higher OI

High oxidized and weathered organic matter.

Higher Si/Ti and biogenic silica

If elevated riverine input of Si, then Si/Ti indicates high precipitation.

Increase in clay minerals

Enhanced weathering and erosion of feldspar-rich rocks

Drier

Lower MS and %clastic

Reduced terrigenous input

Higher TOC

Higher productivity or favorable conditions for organic matter preservation. On its own, does not necessarily indicate dry conditions.

Lower TN and $\delta^{15}N_{bulk}$

Presence of N_2 -fixing cyanobacteria or nitrate-assimilating algae.

Lower C/N

Higher proportion of algae organic matter versus terrigenous sources. On its own not necessarily indicate dry conditions.

Less negative $\delta^{\rm I3} \textbf{C}_{\rm org}$

Indicates a greater proportion of C₄ vegetation from the landscape or increased algal productivity, allowing carbon pool enrichment.

Higher HI

High input of algal or aquatic organic matter.

Lower

Reduced input of easily degradable organic material.

Lower/higher Si/Ti and biogenic silica

Lower values can indicate decreased preservation potential and dissolution of Si in the water column. High values suggest algal bloom under strong upwelling.

Decrease in clay minerals

Shift toward drier conditions

MS: magnetic susceptibility; TOC: total organic carbon; TN: total nitrogen; C/N: carbon:nitrogen ratio; $\delta^{13}C_{org}$: carbon stable isotope; $\delta^{15}N_{bulk}$: nitrogen stable isotope; HI: hydrogen index; OI: oxygen index; OM: organic matter.

in Lake Tanganyika (Felton et al., 2007; Kamulali et al., 2022; Lezzar et al., 2002). That said, the diversity of laminations, particularly in Unit III, leaves open the possibility of underwater currents (possibly lateral, contour-hugging flows) redistributing sediment on the KIR.

Sedimentological and geochemical interpretations

Regarding the statistical analysis, the first two principal components account for ~62% of the total variance (Figure 8). For PC1 (~40% variance), MS, %clastic, C/N, $\delta^{15}N_{bulk}$, and OI vary together and show elevated values when TOC, $\delta^{13}C_{org}$, and HI are relatively low. Therefore, the positive PC1 axis is interpreted to represent an allochthonous sedimentary signal. Strongly positive PC1 values are represented by Unit I-a, the massive blue-gray sediments at the base of core 9B that are interpreted to reflect the products of a wetter hydroclimate. An increase in the MS signal suggests a higher influx of magnetic minerals (e.g. hematite, magnetite, or goethite) from the catchment, which is consistent with enhanced soil erosion and runoff to the lake (Table 2; Thompson et al., 1975). C/N values fluctuate depending on the presence or absence of cellulose in land plant-derived organic matter (Meyers and Ishiwatari, 1993). C/N of 20 or greater suggests the influence of vascular terrigenous sources (Meyers and Ishiwatari, 1993). In contrast, low C/N values (4-10) indicate nonvascular aquatic plants and autochthonous primary production in the water column. Thus, in this case, the directional loading between MS and C/N in PC1 supports an interpretation of allochthonous inputs from the lake's watershed. Elevated values of $\delta^{15}N_{bulk}$ are also consistent with erosion and runoff. Alin et al. (2002) noted that eroded soils from steep watersheds typically result in higher lake sediment δ¹⁵N_{bulk}. Similarly, Talbot et al. (2006) explained that inputs of allochthonous organic matter to Lake Tanganyika from nearby rivers or groundwater flux could also increase $\delta^{15}N_{\text{bulk}}$, while nitrate-assimilating algae or N₂-fixing cyanobacteria

generally result in lower $\delta^{15}N_{bulk}$. Pyrolysis measurements (HI and OI) collectively offer insights into the chemical composition and source of organic matter (McCarthy et al., 2011). The OI values are linked to the oxygen content in kerogen and are often associated with weathered or degraded organic matter (Peters, 1986). Plotting the data on a modified Van Krevelen diagram (Figure 6), Type III kerogens (terrigenous plant materials) are characterized by low HI and high OI values, supporting our interpretation of the positive PC1 trend.

On the other hand, the negative loading of PC1 is interpreted as an indicator of autochthonous primary production under a relatively cool and drier paleoclimate. High TOC values alone do not necessarily indicate a drier climate. However, in Lake Tanganyika, relatively cool and dry conditions favor seasonal upwelling, which is most pronounced in the austral winter (McGlue et al., 2020). Lake Tanganyika's upwelling system is responsible for vertical nutrient flux and diatom blooms, contributing to higher production and burial of sedimentary organic matter (Corman et al., 2010). Since MS is mostly anti-phased with TOC, reduced concentrations may reflect a dilution effect (Wetzel, 2001). Algal blooms are likewise inferred to be responsible for high values in HI and $\delta^{13}C_{\text{org}}$ and for creating bundles of ooze laminae in the core (cf. Cohen et al., 2006). High HI values indicate the presence of algae, bacteria, or amorphous organic matter (Talbot and Livingstone, 1989), as well as favorable redox conditions for organic matter preservation. Enriched $\delta^{13}C_{org}$ values reflect the rate of photosynthesis by algae during upwelling due to preferential uptake of ¹²C during photosynthesis (Pardue et al., 1976).

PC2 (~22% variance) is interpreted to reflect detrital particle size variations and, therefore, sedimentary processes. Core 9B exhibits a high mean %silt content in most units (>50%), while the mean %clay content is usually relatively low (<17%). On the PC2 axis, %silt and %clay load positively and suggest the influence of gravitational suspension settling of particles from the water column. This depositional process is likely for the KIR,

which is bathymetrically elevated with respect to adjacent basinmargin slopes (Scholz et al., 2003). Fine-grained sediments in deepwater are often associated with hemipelagic suspension settling of organic-rich detritus in Lake Tanganyika (Huc et al., 1990). Conversely, the %sand fraction loads negatively in PC2 and more commonly appears in sediments from the AHP. Offshore sand deposition on the KIR is understudied, but several mechanisms are plausible. One possibility is eolian transport, derived for example from desiccated lake beds or exposed shorelines (Gillette et al., 2004; Vandenberghe, 2013; Washington et al., 2006). In the geological record, wind-blown sands have been shown to accumulate in muddy basins when paleoclimate conditions were conducive to transport (Goslin et al., 2018). Another plausible mechanism is riverine plumes carrying mixed grain assemblages (Huc et al., 1990). Waves and currents may subsequently rework these sediments into offshore environments, where settling from the water column occurs along with autochthonous biogenic material. More research is needed to clarify the unexpectedly high %sand concentrations encountered on the KIR. We note that microscopic and X-ray diffraction analyses did not encounter diagenetic minerals that might contribute to %sand measurements.

Infrared spectroscopy has not previously been applied to assess the mineral components in Lake Tanganyika. Amorphous kaolinite, illite-muscovite, and opal populations dominate the composition of core 9B (Figure 5). Amorphous kaolinite is consistently high throughout core 9B, and previous sedimentary records from the northern basin of Lake Tanganyika showed that kaolinite is the major component of clays in the lake sediments, with an average relative abundance of 52%, which is similar to modern soils from the lake basin (Baltzer, 1991). The presence of kaolinite in core 9B suggests that clay minerals from deeply weathered soils have been eroded and transported to the lake basin (Ivory et al., 2021; Velde and Meunier, 2008). Conversely, the proportions of illite-muscovite and opal show greater proportional changes on the KIR during the Middle and Late Holocene. Given the warm and wet paleoclimate of the AHP, we interpret that total clay mineral content provides a more reliable indicator of chemical weathering intensity in core 9B than kaolinite alone.

Termination of the African humid period

Unit I sediments were deposited during (Unit I-a) and immediately following (Unit I-b) the termination of the AHP. Sediments dated to the AHP elsewhere in Lake Tanganyika usually consist of massively bedded, blue-gray clayey silt (Felton et al., 2007; Kamulali et al., 2022). Data from Unit I suggest that the wet and warm conditions of the AHP concluded by ~4600 cal yr BP. The stratigraphy of core 9B suggests a gradual transition rather than a rapid shift to drier conditions at ~4700 cal yr BP shortly after a thermal maximum at ~5000 cal yr BP (Tierney et al., 2008). It is important to note that differences in the temporal resolution of paleorecords and the time-transgressive nature of the AHP termination in lower latitudes contribute to differences in the termination of the AHP among different sites (Shanahan et al., 2015). The AHP is known to have had considerable influence on the paleohydrology of Lake Tanganyika. The overflow of Lake Rukwa into Lake Tanganyika through the Ifume River was demonstrated by paleo-shoreline deposits (i.e. the Ilyandi Sand Ridge) found ~200 m above the modern Rukwa lake level, which were deposited in the Late Pleistocene to Early Holocene (Cohen et al., 2013). The regression of Lake Rukwa is characterized by fossiliferous shoreline terraces at lower elevations from the early Holocene period (~8500-8300 cal yr BP) (Cohen et al., 2013), and the onset of saline conditions began ~5500 cal yr BP, under dryer hydroclimate conditions (Barker et al., 2002; Haberyan, 1987).

Our records suggest that siliciclastic deposition on the KIR was affected by chemical weathering of the surrounding landscape and transport of allochthonous sediments to the lake via riverine plumes during the AHP. Tierney et al. (2008) used compound-specific hydrogen isotopes (δD) and the TEX₈₆ (tetraether index of 86 carbon atoms) temperature proxy to suggest that Lake Tanganyika experienced enhanced summer monsoon rainfall and strong outflow through the Lukuga River at the end of the AHP. We interpret the high MS, kaolinite, illite, and %silt + %clay content of sediments deposited in Unit I to be hallmarks of chemical weathering and erosion, such as would be expected with a high precipitation/evaporation (P/E) condition (Ivory et al., 2021). In core 9B, high C/N and $\delta^{15}N_{bulk}$ are consistent with contributions of terrigenous vegetation to the pool of organic matter and suggest the influence of eroded soils on lake sedimentation (McGlue et al., 2022; Talbot et al., 2006). The $\delta^{13}C_{org}$ values from this interval are consistent with extensive C₃ vegetation in the watershed, which likely flourished under elevated P/E (Ivory et al., 2014). The abundance of amorphous kaolinite in the FTIR dataset supports the interpretation of leached soils in the watershed, resulting in the production and transport of clay minerals to the lake basin (Ivory et al., 2021). By analogy, kaolinite and illite at Lake Malawi are associated with the intense chemical weathering of the highlands surrounding the lake, particularly when forests are present (Ivory et al., 2021).

Unit I-b (~4640–3680 cal yr BP) comprises sediments deposited following the end of the AHP; bedding contacts suggest a gradual transition and the deposition of brown laminated sediments indicates a shift in seasonal conditions. Within Unit I-b, TOC, TN, and HI increase toward the contact with the overlying unit, which we interpret as increasing primary production from phytoplankton and organic matter burial (Talbot et al., 2006). Values of $\delta^{13}C_{\rm org}$ indicate a mixed influence of terrigenous C_3 plants plus algae, which is consistent with values of HI and C/N. We hypothesize that nutrient loading occurring in Lake Tanganyika during the AHP helped to drive this in situ primary production. Cohen et al. (2006) noted that periods of higher precipitation result in P loading in Lake Tanganyika's hypolimnion; strong seasonal winds and upwelling allow these nutrients to be circulated into the photic zone (McGlue et al., 2020).

Late Holocene (~3680-1100 cal yr BP)

Low MS values in the Unit II sediments suggest dominantly carbonaceous sedimentation by hemipelagic settling, with reduced contributions of allochthonous material from the surrounding landscape. Winds at this time may indeed have been strong, as diatom-inferred conductivity in Lake Tanganyika (Figure 9) suggests strong winds under a drier climate (Stager et al., 2009). We interpret that a relatively cool and dry climate prevailed during the deposition of Unit II and extended until ~1100 cal yr BP (within Unit III). In Unit II, the TOC, TN, HI, and $\delta^{13}C_{org}$ shift toward higher values, while $\delta^{15}N_{\text{bulk}}$ shifts lower, suggesting an increase in autochthonous organic matter production. Tierney et al. (2008) interpreted depleted values of δD_{wax} starting ~5000 cal yr BP to reflect a decrease in monsoon activity, as well as a decrease in water temperatures in Lake Tanganyika to ~26°C. In the Late Holocene, pollen records for the Lake Tanganyika basin also show a transition to an environment dominated by thickets and dry miombo under a weakened monsoon (Ivory et al., 2021).

In Unit II, FTIR-inferred mineralogy is characterized by a decrease in illite-muscovite and an increase in opal. Illite and muscovite clays are typically formed under moderate temperatures and moderately acidic to neutral pH conditions in the soil weathering profile (Gharrabi et al., 1998). A decrease in the abundance of these minerals is consistent with partial chemical weathering under drier conditions (Kalindekafe et al., 2019), supported

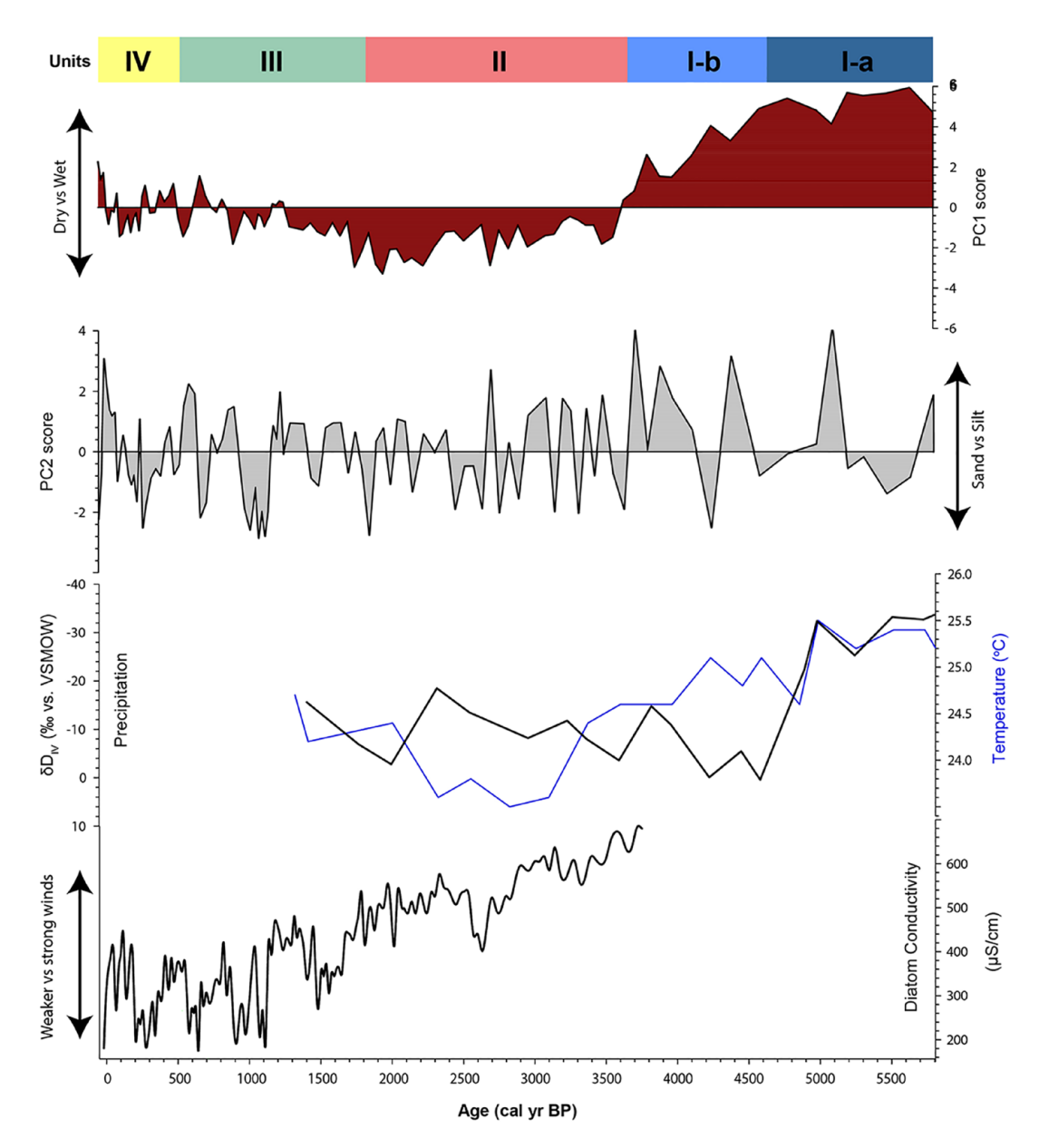


Figure 9. Comparative Holocene datasets from Lake Tanganyika. Results from this study are represented by the PCI (mainly reflecting dry/wet variability) and PC2 scores (reflecting the grain-size variability); TEX86 (lake surface temperature; °C) and δ DIV (‰ vs Vienna standard mean ocean water; indicative of precipitation) are from Tierney et al. (2010b); Diatom conductivity (high conductivity = strong winds and drier conditions) is from Stager et al. (2009).

by other indicators for this period. Opal has an amorphous structure and can be produced by weathering and diagenesis of silicarich rocks or from biological processes, such as in the formation of diatom frustules, sponge spicules, or plant phytoliths (Renaut et al., 2002). The increase in opal is consistent with high autochthonous primary production from diatoms. In addition, the low $\delta^{15}N_{bulk}$ values are consistent with the presence of cyanobacteria, which tend to thrive under conditions of seasonal water column stratification.

Common era

Units III and IV comprise sedimentation during the last two millennia, marked by strong variability in the datasets potentially connected with the Medieval Climatic Anomaly (MCA) and the Little Ice Age (LIA). A high and quasi-cyclic MS signal is apparent in Unit III, with peaks at 48, 36, and 31 cm depth, corresponding to ~1200 cal yr BP (~750 CE), ~1000 cal yr BP (~950 CE), and ~700 cal yr BP (~1250 CE), respectively. The first peak in

MS (~750 CE) is contemporaneous with changes in PC1 score (Figure 9) when the dry and windy conditions begin to give way to a more variable hydroclimate. The latter two MS peaks are associated with the MCA (~950-1250 CE), characterized as a period of warm conditions in the northern high latitudes (Mann et al., 2009). At lower latitudes, the nature and timing of this anomaly are now recognized as spatially complex (Mann et al., 2009). Prior research on Lake Tanganyika sediment cores associated with the MCA suggests wetter conditions from ~800 to 1050 CE that was followed by a period of declining humidity that culminated in drought at ~1150 CE (Alin and Cohen, 2003; Stager et al., 2009). This variable hydroclimate may have contributed to periods of erosion from the landscape. Unit III is also marked by a high %sand content, suggesting contributions of terrigenous grains from the landscape. Laminations in Unit III are the most complex in core 9B and, in some instances, are tilted or discontinuous (Figure 3). It is plausible that bottom-hugging currents may have played a role in the character of these laminations and the transport of sands. From a sedimentological point of view,

only two other studies have explored bedding and laminae characteristics from Lake Tanganyika in detail. Cohen et al. (2006) retrieved cores from the Kalya slope, ~100 km south of our study site, and used laminae thickness to infer the influence of solar activity on sedimentary processes. Those authors interpreted dark laminae couplets and terrigenous-dominated half couplets as lowintensity underflow deposits from riverine sources and light, planktonic diatomaceous ooze, with little terrigenous detritus as windy/dry seasonal deposits (Cohen et al., 2006). In another study, McGlue et al. (2022) investigated laminated carbonaceous sediments from a slope environment adjacent to the Nitiri High in southern Lake Tanganyika. Laminations in that setting were interpreted as an effect of strong seasonal upwelling and associated algal dynamics. The TOC, TN, and HI values remain high in Unit III, with only slight declines compared to Unit II, which attests to continued high productivity and conditions favoring enhanced organic matter preservation.

Previous research suggests that Lake Tanganyika's water level was variable over the Common Era (CE), ranging from ~720 to ~780 m above sea level (asl; Alin and Cohen, 2003), alternating between closed and open basin states and periodic precipitation of CaCO₃ (Haberyan and Hecky, 1987). In Units III and IV, white carbonate laminae are present at different depths, which approximately correspond with carbonate detections in the FTIR dataset (Figure 3b). Calcareous laminae have been reported in other Holocene-age strata in Lake Tanganyika (McGlue et al., 2022; Stager et al., 2009). Haberyan and Hecky (1987) inferred that these laminations reflect the overflow of Lake Kivu via the Ruzizi River, which is responsible for Mg^{2+} and Ca^{2+} delivery to Lake Tanganyika (Cohen et al., 1997b; Craig, 1974; McManus et al., 2015). Deposition of calcium carbonate in Lake Tanganyika appears to have initiated after ~4000 cal yr BP, reflecting connectivity with Lake Kivu (McManus et al., 2015) and supported in this study by the presence of calcite in the FTIR- dataset.

Sediments from Unit IV cover the environmental history of Lake Tanganyika over the last five centuries, which comprise most of the LIA (~1400-1750 CE) for the region (Russell and Johnson, 2007). This unit is marked by the presence of quasicyclic laminated intervals of siliceous oozes and black sapropels (Figure 3a). We attribute these interbedded organic-rich deposits to strong seasonality; diatomaceous oozes accumulate under dry season upwelling, whereas sapropels result from wet season production (Kamulali et al., 2022; McGlue et al., 2022). The geochemistry of Unit IV suggests high primary production under relatively dry and windy environmental conditions, evidenced by high TOC and HI. Stager et al. (2009) interpreted that a brief dry phase occurred at Lake Tanganyika from ~1400 to ~1600 CE, during the inception of the LIA, supported by a low aquatic pollen and a peak in diatom-inferred conductivity. During the LIA, high solar irradiance and La Niña-like conditions in the tropical Pacific Ocean led to strong monsoon winds over Lake Tanganyika, translating into a strong upwelling system and high productivity (McGlue et al., 2020). In Unit IV, the values of $\delta^{13}C_{\rm org}$ continue to be enriched by phytoplankton preferential uptake of ¹²C during photosynthesis. Ivory et al. (2021) suggested that extant climatic conditions stabilized around 1850 CE for this region, marked by an increase in tree pollen and a decrease in grasses. In the late 1800s, lake levels rose, culminating in the 1877 CE opening of the lake, which was followed by a rapid downcutting of the Lukuga River outlet and the stabilization of lake level between 772 and 777 m asl (Cohen et al., 1997b; Evert, 1980).

Conclusions

In this study, we evaluated sedimentary, geochemical, and biogenic indicators from a ¹⁴C-dated sediment core from the KIR to

reveal a more comprehensive history of Lake Tanganyika over the Middle and Late-Holocene.

- The AHP was characterized by an increased riverine discharge into Lake Tanganyika, as indicated by high MS, siliciclastic mass, δ¹⁵N_{bulk}, and FTIR-inferred clay minerals composition. These data suggest an enhanced riverine influx of eroded soils and terrigenous organic matter from the catchment into the lake basin. The unique bluegray clayey sandy silt lithofacies in core 9B and similar facies in other cores across the lake suggest a potential basin-wide sedimentary signal of warm-wet conditions over the AHP.
- Our data suggest a gradual transition out of the AHP, initiated at ~4600 cal yr BP and ended around ~3600 cal yr BP, with a steady decline in precipitation and temperature.
- 3. The enhanced runoff from the AHP was likely responsible for long-term nutrient recharge and loading into Lake Tanganyika, which supported high primary productivity under a relatively cool and dry climate in the middle to Late Holocene (~3680–1100 cal yr BP). Following the transition out of the AHP, laminated silty clays with high TOC and δ¹³C_{org} accumulated on the KIR, indicating elevated phytoplankton primary productivity. The TOC, C/N, Hydrogen Index (HI), δ¹⁵N_{bulk}, and FTIR-inferred opal data suggest the influence of seasonal upwelling.
- 4. The CE is marked by significant variability associated with Late Holocene climatic events. Relatively dry and windy conditions first begin to give way to a more variable hydroclimate around ~1200 cal yr BP (~750 CE), associated with a peak in MS, culminating in a relatively wet hydroclimate around the Medieval Climatic Anomaly. This variable hydroclimate may have contributed to periods of strong erosion from the landscape. Relatively cool and dry conditions of the LIA were marked by the presence of quasi-cyclic laminated intervals of siliceous oozes and bedded black sapropels. Modern hydroclimatic conditions were established around 1850 CE.

Acknowledgements

We thank the Tanzania Commission for Science and Technology for issuing a research permit (permit #16-300-ER-2011-87), the Tanzania Fisheries Research Institute for fieldwork logistical support, and Mupape Mukuli, Joseph Lucas, Athanasio Mbonde, and the crew of *M/V Maman Benita* for fieldwork assistance. We thank the National Lacustrine Core Facility (LacCore) at the University of Minnesota for assisting with the curation of Core 9B and providing a Graduate Visiting Fellowship to the first author. Emma Steiner assisted with granulometric analyses.

Data availability statement

All data generated by USGS laboratories is available in a USGS data release (Birdwell et al., 2024). The remaining data is available upon request from the corresponding author. Any use of trade, firm, or product names is for descriptive purposes only and does not imply endorsement by the U.S. Government.

Funding

The author(s) disclosed receipt of the following financial support for the research, authorship, and/or publication of this article: Funding was provided by the U.S. National Science Foundation (EAR-1424907; EAR-1338553; BoCP-2224886). Additional funding was provided by the University of Kentucky-Pioneer Endowment, the James Roy Maxey Chair in OU Geosciences, SEG-Geoscientists without Borders (201401005), and the Geological Society of America Graduate Research Grant. We acknowledge

the comments and suggestions of Dr. Andrew Cohen, Dr. Jason Flaum, and an anonymous reviewer who helped improve the manuscript's quality.

ORCID iD

Leandro Domingos-Luz D https://orcid.org/0000-0001-8477-

Supplemental material

Supplemental material for this article is available online.

References

- Alin SR and Cohen AS (2003) Lake-level history of Lake Tanganyika, East Africa, for the past 2500 years based on ostracode-inferred water-depth reconstruction. *Palaeogeography Palaeoclimatology Palaeoecology* 199(1–2): 31–49.
- Alin SR, O'Reilly CM, Cohen AS et al. (2002) Effects of land-use change on aquatic biodiversity: A view from the paleorecord at Lake Tanganyika, East Africa. *Geology* 30(12): 1143–1146.
- Baltzer F (1991) Late Pleistocene and recent detrital sedimentation in the deep parts of northern Lake Tanganyika (East African Rift). In: Anadón P, Cabrera L and Kelts K (eds) *Lacustrine Facies Analysis*. Oxford: International Association of Sedimentologists, pp.147–173.
- Barker P, Telford R, Gasse F et al. (2002) Late Pleistocene and Holocene palaeohydrology of Lake Rukwa, Tanzania, inferred from diatom analysis. *Palaeogeography Palaeoclimatology Palaeoecology* 187(3–4): 295–305.
- Birdwell JE, Ellis GE, Wycech JB et al. (2024) Geochemical and spectroscopic data on core samples from Lake Tanganyika in Tanzania. *US Geological Survey Data Release*. DOI: 10.5066/P1GYSKBS.
- Blaauw M and Christen JA (2011) Flexible paleoclimate agedepth models using an autoregressive gamma process. *Bayes-ian Analysis* 6(3): 457–474.
- Burnett AP, Soreghan MJ, Scholz CA et al. (2011) Tropical East African climate change and its relation to global climate: A record from Lake Tanganyika, Tropical East Africa, over the past 90+ kyr. *Palaeogeography Palaeoclimatology Palaeoecology* 303(1–4): 155–167.
- Cohen AS, Gergurich EL, Kraemer BM et al. (2016) Climate warming reduces fish production and benthic habitat in Lake Tanganyika, one of the most biodiverse freshwater ecosystems. *Proceedings of the National Academy of Sciences* 113(34): 9563–9568.
- Cohen AS, Lezzar KE, Cole J et al. (2006) Late Holocene linkages between decade–century scale climate variability and productivity at Lake Tanganyika, Africa. *Journal of Paleolimnology* 36: 189–209.
- Cohen AS, Lezzar K, Tiercelin J et al. (1997a) New palaeogeographic and lake-level reconstructions of Lake Tanganyika: Implications for tectonic, climatic and biological evolution in a rift lake. *Basin Research* 9(2): 107–132.
- Cohen AS, Talbot MR, Awramik SM et al. (1997b) Lake level and paleoenvironmental history of Lake Tanganyika, Africa, as inferred from Late Holocene and modern stromatolites. *GSA Bulletin* 109(4): 444–460.
- Cohen AS, Van Bocxlaer B, Todd JA et al. (2013) Quaternary ostracodes and molluscs from the Rukwa Basin (Tanzania) and their evolutionary and paleobiogeographic implications. *Palaeogeography Palaeoclimatology Palaeoecology* 392: 79–97.
- Corman JR, McIntyre PB, Kuboja B et al. (2010) Upwelling couples chemical and biological dynamics across the littoral and pelagic zones of Lake Tanganyika, East Africa. *Limnology and Oceanography* 55(1): 214–224.

Craig H (1974) Lake Tanganyika geochemical and hydrographic study: 1973 expedition. *Scripps Institution of Oceanography* 75(5): 1–83.

- Degens ET, Von Herzen RP and Wong H-K (1971) Lake Tanganyika: Water chemistry, sediments, geological structure. *Die Naturwissenschaften* 58(5): 229–241.
- DeMenocal P and Tierney J (2012) Green Sahara: African humid periods paced by Earth's orbital changes. *Nature Education Knowledge* 3(10): 12.
- Dreier M and Warden A (2021) Petroleum geochemistry research laboratory programmed pyrolysis method. *US Geological Survey Web Page*. DOI: 10.5066/P9HQSBGH (accessed 22 October 2023).
- Evert MJ (1980) *Le lac Tanganyika, sa Faune et la Peche au Burundi.* Université du Burundi, Bujumbura.
- Felton AA, Russell JM, Cohen AS et al. (2007) Paleolimnological evidence for the onset and termination of glacial aridity from Lake Tanganyika, Tropical East Africa. *Palaeogeography Palaeoclimatology Palaeoecology* 252(3-4): 405–423.
- French KL, Birdwell JE and Lillis PG (2023) Geochemistry of the Cretaceous Mowry Shale in the Wind River Basin, Wyoming. *Geological Society of America Bulletin* 135: 1899–1922.
- Gall R, Birdwell J, Brinkerhoff R et al. (2022) Geologic characterization and depositional history of the Uteland Butte Member, Green River Formation, southwestern Uinta Basin, Utah. *Utah Geological Association Publication* 50: 1–26.
- Gharrabi M, Velde B and Sagon J-P (1998) The transformation of illite to muscovite in pelitic rocks: Constraints from X-ray diffraction. *Clays and Clay Minerals* 46: 79–88.
- Gillette D, Ono D and Richmond K (2004) A combined modeling and measurement technique for estimating windblown dust emissions at Owens (dry) Lake, California. *Journal of Geophysical Research: Earth Surface* 109(F01003): 1–23.
- Goslin J, Fruergaard M, Sander L et al. (2018) Holocene centennial to millennial shifts in North-Atlantic storminess and ocean dynamics. *Scientific Reports* 8(1): 12778.
- Haberyan KA (1987) Fossil diatoms and the paleolimnology of Lake Rukwa, Tanzania. *Freshwater Biology* 17(3): 429–436.
- Haberyan KA and Hecky RE (1987) The late Pleistocene and Holocene stratigraphy and paleolimnology of Lakes Kivu and Tanganyika. *Palaeogeography Palaeoclimatology Palaeo-ecology* 61: 169–197.
- Hammer Ø, Harper D and Ryan P (2001) PAST: Paleontological statistics software package for education and data analysis. *Palaeontologia Electronica* 4(1): 9.
- Hogg AG, Hua Q, Blackwell PG et al. (2013) SHCal13 Southern Hemisphere calibration, 0–50,000 years cal BP. *Radiocarbon* 55(4): 1889–1903.
- Huc A, Le Fournier J, Vandenbroucke M et al. (1990) Northern Lake Tanganyika–an Example of Organic Sedimentation in an Anoxic Rift Lake. In: Katz B (ed.) *Lacustrine Basin Exploration Case Studies and Modern Analogs*. Tulsa: American Association of Petroleum Geologists, pp.169–185.
- Ivory SJ, McGlue MM, Ellis GS et al. (2014) Vegetation controls on weathering intensity during the last deglacial transition in southeast Africa. *PLoS One* 9(11): e112855.
- Ivory SJ, McGlue MM, Peterman C et al. (2021) Climate, vegetation, and weathering across space and time in Lake Tanganyika (tropical eastern Africa). *Quaternary Science Advances* 3(100023): 1–13.
- Ivory SJ and Russell J (2016) Climate, herbivory, and fire controls on tropical African forest for the last 60ka. *Quaternary Science Reviews* 148: 101–114.
- Ivory SJ and Russell J (2018) Lowland forest collapse and early human impacts at the end of the African humid period at Lake

Edward, equatorial East Africa. *Quaternary Research* 89(1): 7–20.

- Kalindekafe L, Dolozi M and Yuretich R (2019) Distribution and origin of clay minerals in the sediments of Lake Malawi. In: Johnson T and Odada E (eds) *Limnology, Climatology and Paleoclimatology of the East African Lakes*. London: Routledge, pp.443–460.
- Kamulali TM, McGlue MM, Stone JR et al. (2022) Paleoecological analysis of Holocene sediment cores from the southern basin of Lake Tanganyika: Implications for the future of the fishery in one of Africa's largest lakes. *Journal of Paleolim*nology 67: 17–34.
- Lezzar KE, Tiercelin J-J and Le Turdu C (2002) Control of normal fault interaction on the distribution of major Neogene sedimentary depocenters, Lake Tanganyika, East African rift. AAPG Bulletin 86(6): 1027–1059.
- Mann ME, Zhang Z, Rutherford S et al. (2009) Global signatures and dynamical origins of the Little Ice Age and medieval climate anomaly. *Science* 326(5957): 1256–1260.
- McCarthy K, Rojas K, Niemann M et al. (2011) Basic petroleum geochemistry for source rock evaluation. *Oilfield Review* 23(2): 32–43.
- McGlue MM, Ellis GS, Brannon MA et al. (2022) Sedimentary geochemistry of deepwater slope deposits in southern Lake Tanganyika (East Africa): Effects of upwelling and minor lake level oscillations. *Journal of Sedimentary Research* 92(8): 721–738.
- McGlue MM, Ivory SJ, Stone JR et al. (2020) Solar irradiance and ENSO affect food security in Lake Tanganyika, a major African inland fishery. *Science Advances* 6(41): eabb2191–eabb2198.
- McGlue MM, Lezzar KE, Cohen AS et al. (2008) Seismic records of late Pleistocene aridity in Lake Tanganyika, tropical East Africa. *Journal of Paleolimnology* 40(2): 635–653.
- McManus J, Severmann S, Cohen AS et al. (2015) The sedimentary response to a rapid change in lake level in Lake Tanganyika. *Palaeogeography Palaeoclimatology Palaeoecology* 440: 647–658.
- Meyers PA and Ishiwatari R (1993) Lacustrine organic geochemistry—an overview of indicators of organic matter sources and diagenesis in lake sediments. *Organic Geochemistry* 20(7): 867–900.
- Murphy C, Oliver T and Warden A (2020) Petroleum Geochemistry Research Laboratory (PGRL) attenuated total reflectance fourier transform infrared method. US Geological Survey Web Page. DOI: 10.5066/P91GXWT4 (accessed 22 October 2023).
- Nicholson SE (2022) The rainfall and convective regime over equatorial Africa, with emphasis on the Congo Basin. In: Tshimanga RM, Moukandi N'kaya GD and Alsdorf D (eds) Congo Basin Hydrology, Climate, and Biogeochemistry: A Foundation for the Future. American Geophysical Union, pp.25–48.
- O'Reilly CM, Alin SR, Plisnier P-D et al. (2003) Climate change decreases aquatic ecosystem productivity of Lake Tanganyika, Africa. *Nature* 424(6950): 766–768.
- Oliver T and Warden A (2020) Petroleum geochemistry research laboratory total organic carbon and total carbon method. *US Geological Survey Web Page*. DOI: 10.5066/P9X85HUF (accessed 22 October 2023).
- Olsson IU (1991) Accuracy and precision in sediment chronology. *Hydrobiologia* 214: 25–34.
- Orr W (1981) Comments on pyrolytic hydrocarbon yields in source-rock evaluation. Advances in Organic Geochemistry 1981: 775–787.
- Pardue JW, Scalan RS, Van Baalen C et al. (1976) Maximum carbon isotope fractionation in photosynthesis by blue-green algae and a green alga. *Geochimica et Cosmochimica Acta* 40(3): 309–312.

Peters KE (1986) Guidelines for evaluating petroleum source rock using programmed pyrolysis. *AAPG Bulletin* 70(3): 318–329.

- Renaut RW, Jones B, Tiercelin J-J et al. (2002) Sublacustrine precipitation of hydrothermal silica in rift lakes: Evidence from Lake Baringo, central Kenya Rift Valley. Sedimentary Geology 148(1-2): 235–257.
- Rosendahl B (1987) Architecture of continental rifts with special reference to East Africa. *Annual Review of Earth and Planetary Sciences* 15(1): 445–503.
- Russell JM, Barker P, Cohen A et al. (2020) ICDP workshop on the Lake Tanganyika Scientific Drilling Project: A late Miocene–present record of climate, rifting, and ecosystem evolution from the world's oldest tropical lake. *Scientific Drilling* 27: 53–60.
- Russell JM and Johnson TC (2007) Little Ice Age drought in equatorial Africa: Intertropical Convergence Zone migrations and El Niño–Southern Oscillation variability. *Geology* 35(1): 21–24.
- Schnurrenberger D, Russell J and Kelts K (2003) Classification of lacustrine sediments based on sedimentary components. *Journal of Paleolimnology* 29: 141–154.
- Scholz CA, Johnson TC, Cohen AS et al. (2007) East African megadroughts between 135 and 75 thousand years ago and bearing on early-modern human origins. *Proceedings of the National Academy of Sciences* 104(42): 16416–16421.
- Scholz CA, King JW, Ellis GS et al. (2003) Paleolimnology of Lake Tanganyika, East Africa, over the past 100 kyr. *Journal* of *Paleolimnology* 30: 139–150.
- Shaban SN, Scholz CA, Muirhead JD et al. (2021) The stratigraphic evolution of the Lake Tanganyika Rift, East Africa: Facies distributions and paleo-environmental implications. Palaeogeography Palaeoclimatology Palaeoecology 575: 110474.
- Shanahan TM, McKay NP, Hughen KA et al. (2015) The time-transgressive termination of the African humid period. *Nature Geoscience* 8(2): 140–144.
- Stager JC, Cocquyt C, Bonnefille R et al. (2009) A Late Holocene paleoclimatic history of Lake Tanganyika, East Africa. *Quaternary Research* 72(1): 47–56.
- Talbot MR, Jensen NB, Lærdal T et al. (2006) Geochemical responses to a major transgression in giant African lakes. *Journal of Paleolimnology* 35: 467–489.
- Talbot MR and Livingstone DA (1989) Hydrogen index and carbon isotopes of lacustrine organic matter as lake level indicators. *Palaeogeography Palaeoclimatology Palaeoecology* 70(1–3): 121–137.
- Thompson R, Battarbee RW, O'Sullivan PE et al. (1975) Magnetic susceptibility of lake sediments. *Limnology and Ocean-ography* 20(5): 687–698.
- Tiercelin J-J and Mondeguer A (1991) The geology of Tanganyka Trough. In: Coulter GW (ed) *Lake Tanganika and its Life*. London: Oxford University Press, pp.7–48.
- Tiercelin JJ, Soreghan M, Cohen A et al. (1992) Sedimentation in large rift lakes: Example from the Middle Pleistocene—modern deposits of the Tanganyika trough, East African rift system. *Bulletin des Centres de Recherches Exploration Production Elf-Aquitaine* 16: 83–111.
- Tierney JE, Russell JM and Huang Y (2010b) A molecular perspective on Late Quaternary climate and vegetation change in the Lake Tanganyika basin, East Africa. *Quaternary Science Reviews* 29(5–6): 787–800.
- Tierney JE, Lewis SC, Cook BI et al. (2011) Model, proxy and isotopic perspectives on the East African humid period. *Earth and Planetary Science Letters* 307(1-2): 103–112.
- Tierney JE, Mayes MT, Meyer N et al. (2010a) Late-twentieth-century warming in Lake Tanganyika unprecedented since AD 500. *Nature Geoscience* 3(6): 422–425.

Tierney JE, Russell JM, Huang Y et al. (2008) Northern hemisphere controls on tropical southeast African climate during the past 60,000 years. *Science* 322(5899): 252–255.

- Vandenberghe J (2013) Grain size of fine-grained windblown sediment: A powerful proxy for process identification. *Earth-Science Reviews* 121: 18–30.
- Vanhove MPM, Pariselle A, Van Steenberge M et al. (2015) Hidden biodiversity in an ancient lake: Phylogenetic congruence between Lake Tanganyika tropheine cichlids and their monogenean flatworm parasites. *Scientific Reports* 5(1): 13669.
- Velde BB and Meunier A (2008) The Origin of Clay Minerals in Soils and Weathered Rocks. Berlin: Springer.
- Vincens A (1991) Late quaternary vegetation history of the south-Tanganyika basin. Climatic implications in South Central

- Africa. Palaeogeography Palaeoclimatology Palaeoecology 86(3-4): 207-226.
- Washburn KE and Birdwell JE (2013) Multivariate analysis of ATR-FTIR spectra for assessment of oil shale organic geochemical properties. *Organic Geochemistry* 63: 1–7.
- Washington R, Todd MC, Lizcano G et al. (2006) Links between topography, wind, deflation, lakes and dust: The case of the Bodélé Depression, Chad. *Geophysical Research Letters* 33(9): L09401.
- Wetzel RG (2001) *Limnology: Lake and River Ecosystems*. Gulf Professional Publishing. San Diego: Elsevier.
- Yost CL, Ivory SJ, Deino AL et al. (2021) Phytoliths, pollen, and microcharcoal from the Baringo Basin, Kenya reveal savanna dynamics during the Plio-Pleistocene transition. *Palaeogeography Palaeoclimatology Palaeoecology* 570: 109779.